Enzyme Kinetics of Muscle Glycogen Phosphorylase b

Sam Walcott*,‡,|| and Steven L. Lehman§

Theoretical and Applied Mechanics, 212 Kimball Hall, Cornell University, Ithaca, New York 14853, and Integrative Biology, 3060 VLSB, University of California, Berkeley, California 94720

Received March 21, 2007; Revised Manuscript Received July 23, 2007

ABSTRACT: Interest in the kinetics of glycogen phosphorylase has recently been renewed by the hypothesis of a glycogen shunt and by the potential of altering phosphorylase to treat type II diabetes. The wealth of data from studies of this enzyme *in vitro* and the need for a mathematical representation for use in the study of metabolic control systems make this enzyme an ideal subject for a mathematical model. We applied a two-part approach to the analysis of the kinetics of glycogen phosphorylase b (GPb). First, a continuous state model of enzyme−ligand interactions supported the view that two phosphates and four ATP or AMP molecules can bind to the enzyme, a result that agrees with spectroscopic and crystallographic studies. Second, using minimum error estimates from continuous state model fits to published data (that agreed well with reported error), we used a discrete state model of internal molecular events to show that GPb exists in three discrete states (two of which are inactive) and that state transitions are concerted. The results also show that under certain concentrations of substrate and effector, ATP can activate the enzyme, while under other conditions, it can competetively inhibit or noncompetitively inhibit the enzyme. This result is unexpected but is consistent with spectroscopic, crystallographic, and kinetic experiments and can explain several previously unexplained phenomena regarding GPb activity *in vivo* and *in vitro*.

Glycogen phosphorylase catalyzes the following reaction:

$$(\text{Glycogen})_n + \text{P}_\text{i} \xrightleftharpoons{\text{Phosphorylase}} (\text{Glycogen})_{n-1} + \text{Glucose-1-Phosphate} \quad (1)$$

The study of glycogen phosphorylase (GP[1]) has a long and rich history, starting with the work of the Coris in the 1930s (*1*). There has been a recent renewal of interest in GP because of new theories about its role in energy flux and as a potential target for a treatment for type II diabetes. Shulman and Rothman (*2*) noted that rapid ATP production in the first few milliseconds of exercise in muscle requires glycogenolysis, as ATP and creatine phosphate supplies are inadequate to support the massive increase in ATP demand. They proposed a "glycogen shunt hypothesis" in which the modulation of GP is central. In their model of the glycogenolytic pathway in skeletal muscle, Lambeth and Kushmerick (*3*) showed that glycogenolysis and glycolysis in skeletal muscle are strongly driven by ATP utilization within a cell and that flux through the glycogenolysis−glycolysis pathway is sensitive to GP activity at rest as well as at moderate and maximal levels of ATP utilization. Interest in GP has also increased with the rise in obesity and associated diseases such as type II diabetes. The possibility of making GP-specific drugs to curb the excessive glucose production responsible for hyperglycemia in diabetics has been suggested (*4*, *5*). Also, the glucose-controlled switch between phosphorylase and glycogen synthase in the liver (*6*) and the difference between controls that permit ultrasensitivity to hormone concentrations in the liver and muscle (*7*) have attracted recent attention.

Glycogen phosphorylase activity is controlled both by covalent modification by an enzyme cascade, whereby phosphorylation of the less active form of the enzyme (phosphorylase b) converts it to the more active form (phosphorylase a), and by allosteric modification. The muscle isozyme of phosphorylase b (GPb) may be activated by AMP to 80% (or more) of the activity seen with muscle phosphorylase a (GPa) (the liver isozyme of GPb, however, achieves only 20% of GPa) (*8*). Here, we focus on GPb because the action of effectors is more pronounced on this form than on GPa, and effectors presumably have a similar influence on GPb as they do on GPa, because there is a richer field of data for GPb, and because GPb may itself be important in the first seconds of intense muscle use, before covalent modification is made.

The renewed interest in glycogen phosphorylase, the potential usefulness of simple yet accurate model for use at the systems level, and the large amount of available kinetic data (e.g., *9*−*18*) indicate that a fresh mathematical analysis of GPb kinetics could lead to interesting and exciting results. Here, we take a two-phase approach, modeling in turn the enzyme−ligand interactions and then the internal molecular events of glycogen phosphorylase action, to find a simple new model of GPb. We conclude (1) that ATP and AMP can bind to four sites per enzyme, while P_i can bind to two; (2) that phosphorylase b exists in at least three discrete states,

* To whom correspondence should be addressed. Phone: (802) 656-3820. Fax: (802) 656-0747. E-mail: scw11@cornell.edu.

‡ Cornell University.

§ University of California, Berkeley.

|| Current address: Molecular Physiology and Biophysics, 115 HSRF, University of Vermont, Burlington, VT 05405.

[1] Abbreviations: GP, glycogen phosphorylase; GPb, skeletal muscle glycogen phosphorylase b; MWC, Monod, Wyman, Changeux; KNF, Koshland, Némethy, Filmer.

10.1021/bi7005527 CCC: $37.00
Published on Web 10/02/2007

two of which are inactive; (3) that state transitions are likely concerted; and (4) that ATP can be a weak activator or strong inhibitor, depending on the concentration and chemical environment.

1. MATERIALS AND METHODS

We analyzed the data using two classes of models: continuous state models and discrete state models. We define a continuous state model as any model in which the conformation of the enzyme is not specified. This class of model could accurately describe enzyme kinetics even if the enzyme had hundreds or thousands (or indeed an infinite number) of functionally different conformations. Our continuous state models are generalizations of the use of binding polynomials as models of data (*19*). In Appendix A, we show that a class of ratios of polynomials are continuous state models. We define a discrete state model as any model in which the enzyme is assumed to exist only in a few functionally distinct conformations. A discrete state model is thus a model of the molecular process by which an enzyme performs catalysis. Monod−Wyman−Changeux and Koshland−Nemethy−Filmer models are well-known examples (*20*, *21*).

1.1. Continuous State Models. A continuous state model makes no *a priori* assumptions about the conformation of the enzyme, as opposed to a discrete state model that assumes the enzyme exists only in a few different conformations. Continuous state models require minimal assumptions (rapid achievement of steady state, pseudo first-order kinetics), but finding the correct form of the model requires the number of ligand and effector binding sites on the enzyme (see Appendix A for details). If this information is not known, then this model provides an estimate. We compared candidate models with different effector or ligand binding sites, and when one candidate model fit the data significantly better than another, we rejected the lesser fit. In the case of phosphorylase b, the number and specificity of binding sites is already known, which provided a way to validate our technique.

We also used the continuous state model to estimate error in the data sets. We found a best fit with a continuous state model and calculated the deviations. We then determined whether the distribution was significantly ($p < 0.05$) different from normal, using a univariate omnibus test (*22*). (A normal error distribution allowed us to use a Chi Square test to objectively accept or reject candidate models.) This error is a minimum error (see Appendix A for details). This error estimate is reliable even if the data were collected in different labs and/or presented in ways that potentially amplify error. In cases in which the experimental method used to collect the data had a known error associated with it (e.g., *18*), we were able to validate this technique.

1.2. Discrete State Models. Once we found the continuous state model that adequately fit the data, we compared different candidate discrete state models to find the number of discrete states, their activity, and the nature of their state transitions. We used the error estimate from the continuous state fits to test two-state MWC, two-state KNF, and three-state MWC models with one or two active states (derived as explained in Appendix B). We used a Chi Square test (with significance set at $p = 0.001$) to determine adequate fits. We justify using such a small p value by the fact that error estimated with a continuous state model is a minimum error.

Table 1: Data Sets from Published Literature Used for Model Fits

temp. (°C)	substrate used	AMP range (mM)	substrate range (mM)	points in data set	reference
25[a]	P_i	0.0−0.9	0.5−25	28	Lowry et al. (*13*)
25	G1P	0.0−0.4	0.0−40	135	Sergienko and Srivastava (*17*)
30	P_i		0.1−35	59	Madsen and Shechosky (*12*)
30	G1P	0.0−80		52	Klinov and Kurganov (*18*)

[a] Data collected at 23 and 26 °C.

The best-fit parameter values (equilibrium constants for binding affinities and state transitions) for these discrete state models were variable when we fit a single data set. To better estimate these values, we fit data sets from experiments run in the direction of glycogen formation along with data from experiments run in the direction of glycogen breakdown. With these more restrictive fits, we found less variation in the equilibrium constants, but we could not be quantitative in determining the significance of fits because the data were collected in different labs under different conditions. Some of these rate and equilibrium constants are reported in the literature, which affords us an opportunity to validate this technique.

1.3. Data Selection. From the large literature on the kinetics of GPb, we selected four data sets. For data in the direction of glycogen breakdown, we considered only data generated since 1965, as data sets generated before the introduction of the MWC model (*20*) are often small and summarized in terms of Michaelis−Menten parameters (e.g., *9* and *10*). A more recent advance in the measurement of reaction rate in the direction of glycogen synthesis (*23*) led to more reliable data sets; therefore, we considered only data generated after 1994 in the direction of glycogen synthesis. Furthermore, we chose data collected under conditions of saturating glycogen because GPb typically works under these conditions *in vivo*. As temperature effects are likely to be important in GPb activity, we chose data collected at two different temperatures, 25 and 30 °C. Ideally, we would include all of the data that matched these selection criteria. However, different methods of protein preparation, differences in buffer concentrations, or other differences in experimental techniques between labs are likely to introduce systematic differences between data collected in different labs. Thus, in order for internal consistency, we chose to include data sets from a single lab for each particular experimental condition. The selected data sources are shown in Table 1, and details regarding each set are given in Appendix C.

1.4. Reading Data from Published Figures. We read data from PDF images of published figures, using a program we wrote in Matlab. To estimate the error associated with the reading process, we read one data set (Sergienko and Srivastava's Figure 1 (*17*)) ten times. The standard deviation at each point averaged 0.05 U/0.458 mg enzyme, irrespective of the value of that point. The maximum y value on the plot was 20 U/0.458 mg enzyme; therefore, the average error associated with reading data from the figure was 0.25% of

Table 2: Inhibitor Fits

inhibitor considered	max. number of ligands per enzyme: AMP	P_i	ATP	data set	*p* value[a]
P_i		4	2	Madsen	
control		2	2	Madsen	> 0.05
ATP		2	4	Madsen	
control		2	2	Madsen	$\ll 0.001$
AMP	4	2		Klinov	
control	2	2		Klinov	$\ll 0.001$

[a] The *p* value reported is the probability that given the error in the modified model the control model could account for the data.

Table 3: Error and Error Distributions for Data Sets

data set	error type	σ_{err}	kurtosis	skew	significant[b]
Klinov	percent	2.5%	3.0	−0.59	no
Serg.[a]	percent	2.3%	3.8	0.33	no
Madsen	percent	5.5%	2.8	0.35	no
Lowry	percent	5.3%	4.2	−0.56	no

[a] A constant error of 0.05 U/mg enzyme, from the minimum resolution of reading the published plots, was subtracted from this error. [b] The *p* value represents the probability that the distribution was normal (significance set at $p = 0.05$).

the maximum *y* value. Assuming that we made the same relative error in reading the data from Lowry et al. (*13*), we estimate the absolute error due to the reading process to be 3 V^e_{max}/v and 0.3 V^e_{max}/v for variable ATP and P_i, respectively. Similarly, we estimate the absolute error due to reading data from the figures of Madsen and Shechosky (*12*) to be 0.05 log $v_0/V^e_{max} - v_0$ and of Klinov and Kurganov (*18*) to be 0.00125 mM/min 62 nM protomer.

1.5. Fitting Data. We used a Nelder−Mead simplex method, Matlab's fminsearch function coded in Fortran 90. To ensure that the optimum fit found is the global optimum, we ran numerous optimizations from initial random seeds, reaching each local optimum multiple times, and picked the lowest. This did not guarantee a global optimum, but it greatly increased the probability of finding one.

2. RESULTS

2.1. Continuous State Results. We first used continuous state models to provide estimates of the number of binding sites for each effector, an estimate of the error distribution for each data set, and an upper bound on the number of free parameters that can be determined from the data sets.

2.1.1. Number and Specifity of Binding Sites. We used the continuous state model to predict the number of effector binding sites on the enzyme. We compared fits from models with four ligand binding sites per enzyme to models with two binding sites. We used the data of Madsen and Shechosky (*12*) with ATP and phosphate as the ligands and the data of Klinov and Kurganov (*18*) with AMP as the ligand. We found a significantly better fit with four binding sites per enzyme for ATP and AMP (two binding sites per protomer), while the fit with four phosphate binding sites was not significantly different from the fit with two (see Table 2). Our model therefore predicts that each protomer has two binding sites for ATP and AMP, and only one for phosphate.

For GPb, the number, position, and specificity of binding sites is largely agreed upon, thus providing a means to validate our technique. Ligands may control muscle GPb at five main binding sites per protomer: a regulatory serine-P site, an allosteric effector site, a catalytic site, a nucleoside inhibitor site, and a glycogen storage site. Phosphorylation of the Ser-14 regulatory site brings about both tertiary and quaternary structural changes that make the phosphorylated enzyme (GPa) an active catalyst. Binding of AMP to the allosteric effector site is thought to bring about similar structural changes in the enzyme as phosphorylation, though through somewhat different mechanisms. ATP is also thought to bind to this site, competing with AMP. The catalytic site is at the center of each subunit. The nucleoside inhibitor site binds purine analogues and related heterocyclic ring compounds, such as adenosine, caffeine, NADH, ATP, and AMP at high concentrations. The physiological significance of this site is unknown. The glycogen storage site binds glycogen particles *in vivo* (*8*, *24*, *25*).

Here, we consider only saturating concentrations of glycogen and no phosphorylation of the Ser-14 regulatory site. Therefore, we consider only three of the enzyme's binding sites: the allosteric effector site, the catalytic site, and the nucleoside inhibitor site. Each protomer should have two binding sites for AMP and ATP, the allosteric effector site and the nucleoside inhibitor site. Our results agree with this prediction. Each protomer should have only one binding site for phosphate, the catalytic site. Our results also agree with this prediction.

We tested our method three times, twice comparing the currently accepted model to a model with one less binding site per protomer and once with one more binding site per protomer. In each case, our method gave a result consistent with the currently accepted view of the number and specificity of binding sites on GPb. This finding validates our method.

2.1.2. Error Size and Distribution in the Data Sets. The error distributions estimated using the continuous state model were normally distributed for three of the four data sets. The Sergienko and Srivastava data set deviated from normality due to a (small) error associated with reading data points off a plot: the data set has many points at low reaction velocities; therefore, these small magnitude errors lead to large percent errors. By repeatedly reading points off the plot and calculating the standard deviation of the distributions of these points, we found a small constant error (0.05 U/mg enzyme), which when added, made the error distribution normal.

The minimum error estimates are shown in Table 3. These error estimates are consistent with the observation that a more accurate technique for measuring reaction velocity was used in the more recent experiments (*17*, *18*) than in the older ones (*12*, *13*), hence the roughly 2-fold decrease in error. Klinov and Kurganov report a 3% error for their data, which compares well with the minimum estimate (2.5%) and validates our error estimation technique.

2.1.3. Bounds on the Number of Free Parameters. The continuous state model provides an upper bound to the number of free parameters for a model (see Appendix A for details). A discrete state model with more free parameters than the upper bound is indistinguishable from the continuous state model and will therefore be essentially a curve fit. This upper bound provides a limit on the complexity of any

Table 4: Two and Three State Fits for Data Sets

data set used	states in model	type of model	χ^2_{crit} [a]	χ^2	times from random seeds	significant [b]
Klinov	2	MWC	89.3	151	4	$p < 0.001$
Klinov	2	KNF	89.3	151	6	$p < 0.001$
Klinov	3	MWC	89.3	66.2	2	no
Serg.	2	MWC	192	298	5	$p < 0.001$
Serg.	2	KNF	192	298	10	$p < 0.001$
Serg.	3	MWC	192	117	4	no
Madsen	2	MWC	98.3	308	5	$p < 0.001$
Madsen	2	KNF	98.3	308	5	$p < 0.001$
Madsen	3	MWC	98.3	91.4	6	no
Lowry	2	MWC	56.9	48.8	4	no
Lowry	2	KNF	56.9	46.6	2	no
Lowry	3	MWC	56.9	37.7	4	no

[a] χ^2_{crit} is the χ^2 value at which $p = 0.001$. A χ^2 below that value means an acceptable fit. [b] The p value represents the probability that given the error estimate from the continuous state model the discrete state model considered could have generated the data set.

discrete state model. The upper bound was 14 for the data of Lowry et al. and of Sergienko and Srivastava, and was 24 for the data of Klinov and Kurganov and Madsen and Shechosky. The different upper bounds are due to the different experimental conditions (e.g., presence of ATP or high AMP concentrations) that led to the data sets.

2.2. Discrete-State Results. 2.2.1. GPb Is Adequately Modeled Using Three Discrete States but Not Two. We identified discrete state models that fit the constraints imposed by the continuous state models, a two-state concerted model, a three-state concerted model, and a two-state sequential model. In the following, the concerted models will be denoted MWC, as the assumptions behind them are those of Monod, Wyman, and Changeux, and the sequential model will be denoted KNF, as the assumptions behind it are those of Koshland, Nemethy, and Filmer. For three of the four data sets, the best-fit two-state MWC model generated a series of points that was significantly different ($p < 0.001$) from the experimentally determined points, while the best-fit three-state MWC model generated a series of points that was not significantly different ($p > 0.001$) from the experimentally determined points, given the error estimate from the continuous state model (see Table 4). For the Lowry data set, though the three-state best-fit was better than the two-state fit, the two-state fit was not quite significantly different from the experimental points. The Lowry et al. data had the fewest points; therefore, it seems likely that with more points the difference would become significant.

In order to minimize variation in the parameters of the model, we simultaneously fit the discrete state models to two data sets, one in the direction of glycogen synthesis and one in the direction of glycogen breakdown. The 25 °C data, consisting of Lowry et al. and Sergienko and Srivastava, gave a χ^2 value of 179 ($p = 0.18$) for the three-state fit and a χ^2 value of 394 ($p \ll 0.001$) for the two-state fit. The three-state fit appears to be a good fit to the data, while the two-state fit has some systematic deviations, being unable to match the curvature of the plots correctly (see Figure 1). The 30 °C data, consisting of Madsen and Shechosky, and Klinov and Kurganov, gave a χ^2 value of 201 ($p < 0.001$) for the three-state fit and a χ^2 value of 498 ($p \ll 0.001$) for the two-state fit. Again, the three-state model appears to be a good fit, while the two-state fit has systematic deviations, especially in the Madsen and Shechosky data at high

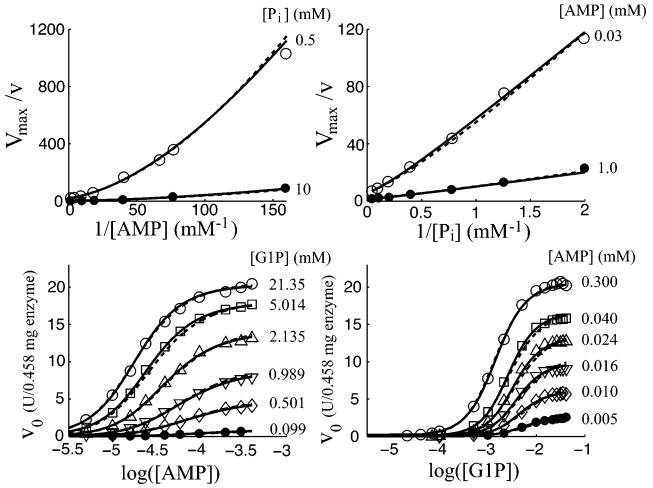

FIGURE 1: Discrete-state fits to data collected at 25 °C. A two-state model (---) and a three-state MWC model (—) was fit to reaction velocity data for muscle GPb in the direction of glycogen breakdown (top) (*13*) and to data in the direction of glycogen synthesis (bottom) (*17*). The plots on the left were generated at constant levels of substrate and variable levels of the activator AMP, while plots on the right had constant AMP with variable substrate. The plots in this figure are presented in the same form as originally published (Lineweaver−Burk for the top and semilog for the bottom). The error bars, as estimated from the continuous state model, are comparable in size or smaller than the symbols on the plots. Note that the small size of the error bars makes the subtle deviations between the two and three-state models significant.

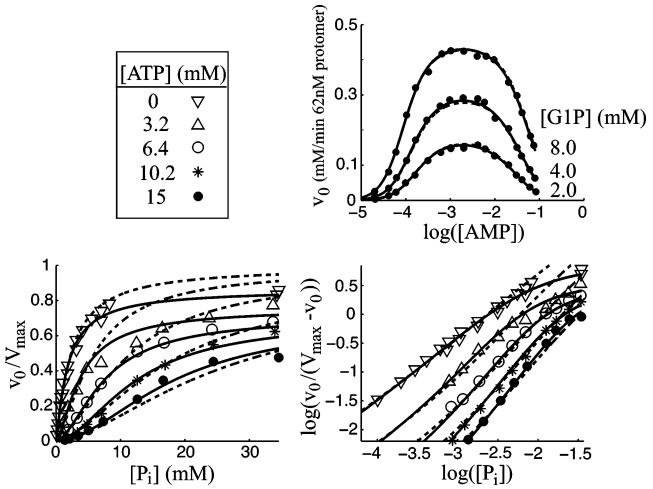

FIGURE 2: Discrete-state fits to data collected at 30 °C. A two-state model (---) and a three-state MWC model (—) was fit to reaction velocity data for muscle GPb in the direction of glycogen synthesis (top) at three different levels of substrate (*18*), and to data in the direction of glycogen breakdown (bottom) at five different levels of the inhibitor ATP in the presence of 1 mM AMP (*12*). The error bars, as estimated from the continuous state model (or from the 3% error reported by Klinov and Kurganov), are comparable in size or smaller than the symbols on the plots. The same parameters were used for the fits to both data sets, though the conditions under which the data were collected were slightly different. The plots on the right are as presented in the original papers, while the plot on the left is in the more traditional form of v/V^t_{max} vs effector or substrate. The legend shows the symbols used for the lower plots.

substrate concentrations (see Figure 2). This deviation is what prompted Madsen and Shechosky to conclude that there could be phosphate inhibition. Thus, it would appear that a third state is sufficient to explain this drop in activity and apparent phosphate inhibition. These results support the

Table 5: Three State, Discrete State Fits to Combinations of Data[a]

data used	SL	KM	SL range[b]	KM range[c]	SL two active	KM two active
$K_{TT'}$	0.202	0.497	1e-4−0.20	7.7e-6−0.50	0.000239	0.294
K_{TR}	1.14e-4	3.4e-8	2.3e-5−1.1e-4	1.4e-9−3.4e-8	1.45e-6	2.79e-6
$K_{T'Aa}$	9.90	8.72	9.9−24	0.54−9.3	21.0	12.2
K_{TAa}	17.7	1.9e-6	17−18	1.9e-6−4.6	17.5	0.542
K_{RAa}	922	2.13e4	920−2000	2.1e4−1.0e5	2.50e4	5810
$K_{T'P_i}$	0.454	0.287	0.0002−0.45	1.5e-5−0.31	1.03	0.369
K_{TP_i}	0.104	0.00172	0.10−0.18	0.001−0.23	0.178	0
K_{RP_i}	0.473	1.34	0.47−0.48	1.1−1.3	0.494	1.59
$K_{T'G1P}$	0.595	0.0327	0.60−23	0−26	13.7	0
K_{TG1P}	0.0	0.0106	0.0−0.056	0−0.040	0.0602	0.0514
K_{RG1P}	1.71	0.425	1.5−1.7	0.36−0.43	1.59	0.630
$K_{T'Ai}$		0.0337		0.020−0.54		0.0139
K_{TAi}		2.65e-6		0.0−0.54		0.550
K_{RAi}		0.0		0.0−0.0034		0.00384
$K_{T'Ii}$		0.0		0.0−25		2.11e-5
K_{TIi}		1.20		0.50−1.2		1.16
K_{RIi}		0.0555		0.045−0.072		0.0463
$K_{T'Ia}$		2.92		0−26		3.15
K_{TIa}		1.20		0.001−1.2		1.11
K_{RIa}		1190		1200−7900		272
k_R	77.2	94.1	77−86	86−94	84.2	79.8
$k_{T'}/k_R$					0.0225	0.336
χ^2	179	201	179−187	201−208	176	195

[a] See Appendix B for the definition of parameters. Concentrations are in millimolar, and time is in seconds. [b] KM, (*18*, *12*); SL, (*17*, *13*). [c] Represents the range of parameters for the best local minima.

conclusion that a two-state model is inadequate for modeling GPb, while a three-state MWC model with two inactive states is adequate. The more modern data sets (with smaller error) and the data sets with more points all supported the conclusion that a three-state MWC model could have produced the data, while a two-state model (either MWC or KNF) could not.

To test the hypothesis that two of the three states in the model are inactive, we modified the model to allow two active states and thus added a new parameter to the model: the ratio of the rate constants of the two active states. These fits generated the same best-fit parameters to the combinations of data as the previous model. We also found two additional fits, one for each temperature, which had two semi-active states. For the Sergienko−Lowry (25 °C) fit, the activity was very small (less than 4% of the activity of the most active state). For the Madsen−Klinov fit (30 °C), the value of k_R was outside the range measured in experiment. Additionally, the parameters of this fit (except k_R) were not very different from the previously found fits (see Table 5). In both cases, these fits with semi-active states were not much better than the fits with inactive states (χ^2 values of 176 and 195 compared to 179 and 201 for the 25 °C and 30 °C data, respectively) so that it seems likely that two inactive states is a valid assumption.

2.2.2. State Transitions Appear to Be Concerted. A MWC model is a special, simplified case of a KNF model, having two fewer parameters as explained in Appendix B. For all of the data sets except for those of Lowry et al., the simplest model that could explain the data was the three-state MWC model. For the data of Lowry et al., the two-state MWC model fit the data adequately. Therefore, the simplest model that could fit the data had concerted state transitions.

2.2.3. ATP Can Be a Weak Activator or Strong Inhibitor of GPb. Our three-state model predicts that ATP can either inhibit or activate GPb by mechanisms that are consequences of having two binding sites per protomer for ATP (from the continuous state model fit) and of having two inactive states (from the discrete state model fit). The model predicts that ATP activates GPb by binding to the allosteric site, as AMP does, but with much lesser affinity. Our parameter estimates would make ATP a weak activator, useful only at low [AMP] (see Table 5). When it binds at the nucleoside inhibitor site, ATP would act as an inhibitor by shifting the equilibrium from one inactive state (T'), which is the most occupied state when AMP is bound to the allosteric site, to the other inactive state (T), a state with low affinity for AMP. Thus, the model allows for a range of control by [ATP], from weak activation when [AMP] is low to strong inhibition when [AMP] is high. In addition to the balance between [AMP] and [ATP], the binding of ATP to the nucleoside site also depends on [P_i], according to the model's predictions. ATP would inhibit at physiological concentrations when [P_i] is low, as in resting muscle, but not when [P_i] is high, as in fatigued muscle.

2.2.4. Testing the Fits. The lower the number of free parameters in a discrete state model, the lower the likelihood that a model that fits the existing data is simply a good curve-fit. The continuous state model provides an upper bound to the number of free parameters. If this upper bound is exceeded, then the discrete state model is indistinguishable from the continuous state model, and the parameters have ambiguous physical meaning. Thus, the model with the fewest parameters with respect to this upper bound, yet can still adequately fit the data, is most likely to provide insight into enzyme function. For the Lowry et al. data and the Sergienko and Srivastava data, the maximum number of free parameters was 14. The three-state model for both data sets required 8 parameters. For the Klinov and Kurganov data and the Madsen and Shechosky data, the maximum number of free parameters was 24, while the three-state model required 11. In all cases, the number of free parameters was well below the maximum.

To further ensure that the best-fit discrete state models were not simply curve-fits, we looked at some of the

predictions of the best-fit parameters and compared them to previously measured values. The simplest parameter to be tested is k_R, the rate constant for the reaction of enzyme−substrate to product in the direction of glycogen synthesis. Measured values of k_R at 25 °C range from 68.55−79.9 s^{-1} (*17*, *26*), while our best fit values ranged from 77.2−86.5 s^{-1}. Measured values of k_R at 30 °C range from 84−114 s^{-1} (*16*, *18*, *10*), while our best-fit values ranged from 85.8−94.1 s^{-1}. Note that we would expect the theoretical values to be larger than the measured values since the theoretical value is the upper possible limit, and the measured value only approaches that limit. The reasonably good agreement between our model and experiment as well as the consistency of our parameters suggests that we did not simply do a curve-fit to the data.

3. DISCUSSION

Glycogen phosphorylase is "one of the most carefully studied proteins in existence" (*27*). As a result, it would seem likely that a clear description of its action *in vivo* should exist; but there is no widely accepted model that can explain all of the data. For example, some research has suggested that GP can exist in two discrete states with sequential (in GPb) or concerted (in GPa) state transitions (see *24*), yet it has been shown repeatedly that a two-state model cannot explain the kinetic data (*13*, *15*, *16*). Structural evidence has pointed to discrete-states for GPa and GPb (*8*), yet most current models are continuous state models (*18*, *26*). It is well accepted that ATP binds to four sites per enzyme (*24*), yet it is also well accepted that AMP and ATP interact through (classic Michaelis−Menten) competitive inhibition (*9*, *10*). All of these contradictory results point to one clear conclusion: GPb can behave in counterintuitive ways. Here, we present a model that can explain all of the available data. We now discuss the four results from the model (number and specificity of binding sites, discrete states, concerted state transitions, and the action of ATP and AMP), paying careful attention to incorporate as much data from as many experiments as possible.

3.1. Binding Sites. The continuous state model fits to the data suggested that there are 2 (not 4) binding sites for phosphate, 4 (not 2) binding sites for ATP, and 4 (not 2) binding sites for AMP per enzyme. None of these results is surprising, given the current view of enzyme structure. We expect that ATP and AMP bind to the nucleoside inhibitor and allosteric effector sites; since there are two subunits per enzyme, this would predict 4 sites per enzyme for both. We expect that P_i binds exclusively to the active site (at physiological concentrations), predicting 2 sites per enzyme. Thus, the determination of binding sites supports the current view of GPb and validates our approach.

3.2. Discrete States. We were unable to fit most (3/4) of the data sets with a two-state model, and we fit all of the data sets with a three-state model. The one data set that was fit adequately with a two-state model was the smallest and one of the oldest (and thus the most uncertain). The clearest conclusion is that a discrete state model can fit the available data. Any continuous state model does not take advantage of the simplifications (i.e., fewer free parameters) that can be afforded by a discrete state model. Therefore, any insights that can be gained from the parameters of a discrete state model are hidden in the more complicated continuous state models.

Another conclusion we may make is that GPb exists in three discrete states, two of which are inactive. We know of no three-state model with two inactive states; Kastenschmidt et al. (*15*) propose the only other three-state model of which we are aware, but their model has two equally active states. Crystallization studies have only identified two states, not a surprising result in light of the scarcity of the active *R* state. It is possible that the two crystallized states are the inactive *T* and *T′* states. We could then explain why two-state models have failed to fit kinetic data (since a third state is necessary) and why the catalytic mechanism for GPb has remained elusive (since what is called the active *R* state in the structural literature is in fact what we call the inactive *T′* state).

3.3. Concerted State Transitions. We found that a three-state MWC model fit each data set adequately, while a two-state KNF model was unable to fit most data sets. We conclude that the existing evidence suggests state transitions are concerted in GPb. This model is the simplest one that can explain all of the data. We know, however, that a three-state KNF model could also explain all of the data. It is possible that with more exact data the three-state MWC model could be rejected. Until those data exist, the simplest model is assumed to be correct.

The current view of the nature of state transitions in GPb is unclear, with some evidence suggesting that state transitions are concerted (in that when one protomer changes conformation, the other follows suit immediately) (*28*, *29*) and other evidence suggesting that the transitions are sequential (in that hybrid states exist, where the protomers are in different conformations) (*24*, *30*, *31*). Using structural evidence to infer whether state-transitions are concerted is problematic because the hybrid state should exist for some short time even in an enzyme that is well-modeled as having discrete state transitions. Thus, we really want to know whether these hybrid states contribute significantly to the reaction rate. A particular state's contribution to reaction rate can be measured most readily in kinetic studies rather than in static structural studies. The presence of a third state may also have led to the lack of consensus regarding whether the state transitions of phosphorylase are concerted or not in that the apparent transition state (that the authors interpret as the hybrid state in the KNF model) may in fact be the third state.

3.4. Action of AMP and ATP. AMP and ATP can bind to both the allosteric activator site or the nucleoside inhibitor site of each phosphorylase subunit, depending on concentrations. This finding explains the well-known observation that AMP inhibits phosphorylase at nonphysiological concentrations (above 2 mM). Activation occurs by AMP binding in an inactive state and leading to a transition to the active state. This mechanism is consistent with the observation that AMP binding does not necessarily result in a transition to the active state (*24*). AMP inhibition at high concentrations (above 2 mM) works by low affinity binding to the nucleoside site in the *T′* state.

The prediction that ATP can inhibit GPb by binding to the nucleoside inhibitor site as well as the prediction that ATP can activate GPb is contrary to the conventional view of ATP as a competitive inhibitor but may not be contrary to the data that led to that view. The classic kinetic evidence

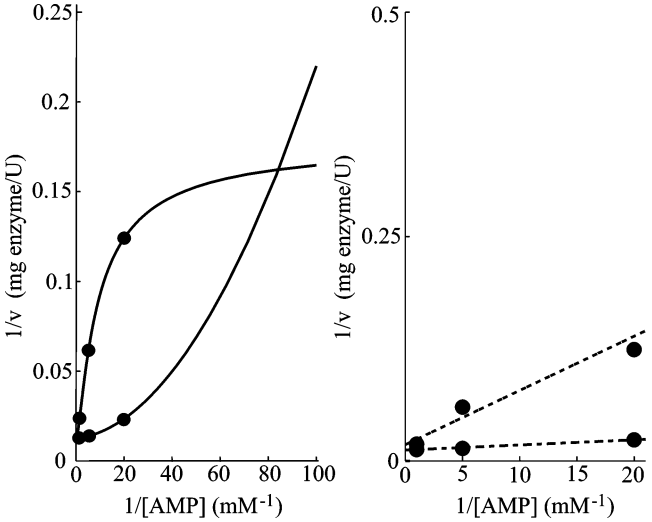

FIGURE 3: Is ATP a competitive inhibitor? The left plot shows a double reciprocal plot of velocity and AMP at 24 mM G1P in the direction of glycogen synthesis, at 0 ATP (upward curving) and 4 mM ATP (downward curving). Both plots are clearly nonlinear, indicating that non-Michaelis−Menten kinetics occur. The right plot shows a restricted window of the left plot with only three data points, as used in refs *9* and *10*, and two linear fits to the data. The linear fits appear good, though it is clear from the left plot that the graphs should be nonlinear. Thus, we argue that it is possible that the kinetic evidence for ATP as a purely competitive inhibitor with AMP for the allosteric activator site may in fact not exclude different forms of inhibition, as predicted by our model.

for competitive inhibition by ATP is based on double reciprocal plots of AMP and velocity, with G1P as substrate and assumed Michaelis−Menten kinetics (*9*, *10*). However, since GPb does not obey Michaelis−Menten kinetics, simple graphical methods of determining ligand interactions are not so easily applicable. Our model can generate apparently linear double-reciprocal plots over the range used in the kinetic studies (*9*, *10*) even though, if taken over a wider range including small AMP concentrations, the actual curves are far from linear (see Figure 3). As further kinetic evidence for AMP and ATP competition for the same binding site, some authors have pointed out that increasing AMP concentration tends to eliminate the inhibition by ATP (*9*). Our model also shows this effect. The spectroscopic work of Busby and Radda (reviewed in (*32*)) has provided further evidence for competitive inhibition for ATP and AMP (and also ADP). But they do not distinguish between inhibition where ATP and AMP bind to the same site or inhibition where ATP binding to a separate site leads to a transition into a state where AMP cannot bind. Our model predicts that ATP has almost no affinity for the nucleoside site when the enzyme is in the *T*′ state and that AMP has almost no affinity for the allosteric activator site when the enzyme is in the *T* state (see Table 5) and thus agrees with this experiment.

The structural evidence for competitive inhibition is based on crystallizing the enzyme with ATP bound and comparing that structure to the enzyme with AMP bound (*33*, *34*). However, this method only gives information about the lowest energy conformation of the enzyme. According to our parameters, even with two molecules of AMP bound, the most common form of the enzyme will be the *T*′ state and not the active *R* state. The enzyme with two molecules of ATP bound will favor the *T* state to a much larger extent. Thus, the enzyme with ATP bound can be in a different conformation than enzyme with AMP bound, even though both ATP and AMP activate the enzyme. Our parameters also predict that ATP binds more strongly to the allosteric activator site than the nucleoside inhibitor site and that ATP has a higher affinity for the nucleoside inhibitor site than AMP. Both of these predictions are in agreement with structural experiments (*25*).

Our model that includes both activation and inhibition by ATP would explain three otherwise puzzling observations. First, ADP is thought to act in a manner similar to that of ATP, competing with AMP for the allosteric activator site (*32*), but recent kinetic studies of Rush and Spriet have shown that ADP alone has an *activating* effect on GPa in the absence of other effectors (*35*). Assuming that GPa reacts to effectors in a manner similar to that of GPb, this observation makes sense in light of our model. At low concentrations in the absence of other effectors, ADP (if it works like ATP) is a weak activator, while at higher concentrations, the action of ADP turns inhibitory. In the presence of AMP, ADP is inhibitory, and since most studies on GPb are done with relatively large concentrations of AMP, the action of both ATP and ADP appear inhibitory. Second, rats lacking muscle phosphorylase kinase (and thus possessing only GPb) are essentially asymptomatic (*36*). If ATP activation occurs, then maybe ATP activates GPb enough for glycogenolysis to function. Third, creatine kinase (CK) deficient rats show an increase in GPb activity (*37*). ATP hydrolysis in a CK deficient muscle should cause increases in [P_i] and [ADP], both of which activate GPb according to our model.

3.5. Predictions. The model predicts that ATP at low concentration should be a weak activator of GPb in the absence of AMP. This activity, though small, might be measurable using a sensitive technique, for example, that of Sergienko and Srivastava (*23*).

The model predicts three functionally distinct states of GPb, though only two structures have been crystallized. Because it is based on kinetic and not structural data, the model does not suggest structural experiments. However, spectroscopic techniques might reveal different conformations under conditions favoring the different states. The parameters of our model predict that under conditions of activating AMP (1 to 2 mM) and saturating P_i (30−50 mM) at 25 °C, about 85% of the enzyme should be in the *R* state. Under slightly lower conditions of AMP (0.75 mM) but no P_i, we predict that at 25 °C about 75% of the enzyme should be in the *T*′ state. Under conditions without AMP or P_i but saturating ATP (above 10 mM) at 25 °C, the enzyme should be almost exclusively (> 98%) in the *T* state.

3.6. Conclusions. We have presented a method for modeling enzyme kinetics. We use a two-phase approach. First, we found the best-fit continuous state model, which in its most general form has 48 parameters (eq 8 in Appendix A, with $s = 2$, $r = 4$, and $q = 4$). We used this result to infer the following: (1) that GPb had four binding sites for ATP and AMP with only two binding sites for P_i; (2) the average error as well as the distribution of that error; and(3) an upper bound on the number of free parameters. Since the kinetics of GPb have been studied extensively, we were able to compare our model results for binding site number and

specificity as well as our error estimate to experimentally determined values. The agreement was good, validating this method. Second, using the constraints imposed by the continuous-state model, we found the best-fit discrete state model: a three-state MWC model that in its most general form has 18 parameters. (The model may be derived as described in Appendix B.) We used this result to infer that (1) GPb must have at least three discrete states; (2) state transitions are concerted; and (3) ATP and AMP can be activators or inhibitors depending on concentration, though ATP is a weaker activator and a more potent inhibitor. Our three-state model is supported by kinetic data, though at present structural studies have only identified two states. That our model has concerted state transitions adds support to one side of a debated issue. Our interpretation of the action of effectors is new but consistent with previous studies. Furthermore, it can explain some puzzling observations regarding GPb action *in vivo*. More detailed discrete state models, as presented here, should be of great use in predicting the results of experiments, creating more exact system-level models of metabolism, and in designing new and effective methods of treatment for disease.

4. APPENDIX A

Ratios of polynomials are generally useful for approximating functions (i.e., a Padé approximation) because they can sometimes fit better than polynomials with the same number of coefficients. Their use in enzyme kinetics dates from the late 1950s and early 1960s (*38*−*40*) and was well developed by Bardsley and Childs (*41*), who showed that many common curves relating rate of product production as a function of ligand concentration could be produced by ratios of polynomials with positive coefficients. Childs and Bardsley derived some general properties of this subclass of rational polynomials and showed how velocities of some discrete state allosteric models could be developed as ratios of polynomials, with the polynomial coefficients given in terms of the parameters of the discrete state model (*42*).

Here, we show that if the coefficients of these polynomials are chosen independently, a continuous state model is assumed. The rate at which an enzyme catalyzes a reaction can depend on concentrations of substrate and of other ligands and on the conformational state of the enzyme. Assuming that enzyme in different conformations and combinations of ligands may produce product at some rate, the overall rate of catalysis must be the sum of these individual rates, each multiplied by the probability of finding the enzyme in the given conformation with the given number of ligands bound.

Assume an enzyme has r binding sites for ligand (not substrate) L and s binding sites for substrate S. The enzyme's different conformations can be measured by some vector x of arbitrary length (e.g., a vector of the bond rotations and bond lengths of the enzyme), and an arbitrary reference conformation can be assigned the value $\mathbf{x} = \mathbf{0}$. If the reaction $E(\mathbf{0}) + iL + jS \rightleftharpoons E(\mathbf{x})L_iS_j$ is in steady state and obeys pseudo-first-order kinetics, then we may write $[E(\mathbf{x})L_iS_j] = K_{ij}(\mathbf{x})[E(\mathbf{0})][L]^i[S]^j$; then the probability density (ρ) at equilibrium of $E(\mathbf{x})L_iS_j$ is as follows:

$$\rho(E(\mathbf{x})L_iS_j) = \frac{[E(\mathbf{x})L_iS_j]}{[E_{tot}]} = \frac{K_{ij}(\mathbf{x})[E(\mathbf{0})][L]^i[S]^j}{[E_{tot}]} \quad (2)$$

where $[E_{tot}]$ is the total concentration of enzyme in solution. In this equation, we have assumed that enzyme−substrate binding is in steady state. The rate density of production of product from this enzyme−ligand−substrate combination is $v_{ij}^{max}(\mathbf{x})$ times this probability density, where $v_{ij}^{max}(\mathbf{x})$ is the rate of catalysis that would occur if all the enzyme were $E(\mathbf{x})L_iS_j$. Thus, if the enzyme conformation-dependent rate constant is $k(\mathbf{x})$, then $v_{ij}^{max}(\mathbf{x}) = jk(\mathbf{x})[E_{tot}]$. The overall rate of the catalyzed reaction would be the sum of the rates of production of all of the enzyme−ligand−substrate possibilities:

$$v = \int_{\mathbf{x}} \sum_{i=0}^{s} \sum_{j=1}^{s} jk(\mathbf{x})K_{ij}(\mathbf{x})[E(\mathbf{0})][L]^i[S]^j d\mathrm{x} \quad (3)$$

The theoretical maximum rate of catalysis would occur if every enzyme were in the conformation with the largest velocity, saturated with substrate.

$$V_{max}^t = max(v_{ij}^{max}) = s||k(\mathbf{x})||_{L_\infty}[E_{tot}] \quad (4)$$

We append the superscript t to this definition of V_{max} in order to distinguish it from the maximum velocity extrapolated from kinetic data, which we designate V_{max}^e. It is usually assumed that V_{max}^e which is an approximation of enzyme velocity at large substrate and activator concentrations (typically from a Lineweaver−Burke plot) is equal to V_{max}^t; however, since substrate and activator may be inhibitory at large concentrations and since V_{max}^e may indeed never approach V_{max}^t, we choose to keep them separate.

The relative rate would then be given by

$$\frac{v}{V_{max}^t} = \frac{\int_{\mathbf{x}} \sum_{i=0}^{r} \sum_{j=1}^{s} jk(\mathbf{x})K_{ij}(\mathbf{x}))[E(\mathbf{0})][L]^i[S]^j d\mathrm{x}}{s||k(\mathbf{x})||_{L_\infty}[E_{tot}]} \quad (5)$$

We can write $[E_{tot}]$ in terms of equilibrium constants and the concentration of enzyme in the reference conformation as follows:

$$[E_{tot}] = \int_{\mathbf{x}} \sum_{i=0}^{r} \sum_{j=0}^{s} K_{ij}(\mathbf{x})[\mathrm{E}(\mathbf{0})][\mathrm{L}]^i[\mathrm{S}]^j d\mathbf{x} \quad (6)$$

Plugging this into eq 5 and simplifying results in the following equation:

$$\frac{v}{V_{max}^t} = \frac{\int_{\mathbf{x}} \sum_{i=0}^{r} \sum_{j=1}^{s} K_{ij}(\mathbf{x}) \frac{jk(\mathbf{x})}{s||k(\mathbf{x})||_{L_\infty}} [L]^i[S]^j d\mathbf{x}}{\int_{\mathbf{x}} \sum_{i=0}^{r} \sum_{j=0}^{s} K_{ij}(\mathbf{x})[L]^i[S]^j d\mathbf{x}} \quad (7)$$

This relationship generalizes easily. For two ligands L and M, the numerator in eq 7 would become $\int_{\mathbf{x}} \sum_{w=0}^{q} \sum_{i=0}^{r} \sum_{j=1}^{s} K_{wij}(\mathbf{x})(jk(\mathbf{x})/s||k(\mathbf{x})||_{L_\infty})[L]^i[M]^w[S]^j d\mathbf{x}$, and the denomi-

nator, a form of the binding polynomial (*19*, *43*), would become $\int_{\mathbf{x}}\sum_{w=0}^{q}\sum_{i=0}^{r}\sum_{j=0}^{s}K_{wij}(\mathbf{x})[L]^i[M]^w[S]^j d\mathbf{x}$. The relationships between the coefficients $K_{wij}(\mathbf{x})$ would capture cooperativity between ligand bindings in a certain enzyme conformation. For example, positive cooperativity for ligand L in the conformation x_0 would be represented by $K_{wij}(\mathbf{x}_0) > K_{wi-1j}(\mathbf{x}_0)$.

The most general form of the relative rate equation (eq 7) we will use is

$$\frac{v}{V^t_{max}} = \frac{\sum_{w=0}^{q}\left(\sum_{i=0}^{r}\left(\sum_{j=1}^{s}C_{wij}[S]^j\right)[L]^i\right)[M]^w}{\sum_{w=0}^{q}\left(\sum_{i=0}^{r}\left(\sum_{j=0}^{s}D_{wij}[S]^j\right)[L]^i\right)[M]^w} \qquad (8)$$

where we have evaluated the integral over the enzyme conformations, setting $C_{wij} = \int_x K_{wij}(\mathbf{x})(jk(\mathbf{x})/s||k(\mathbf{x})||_{L_\infty})d\mathbf{x}$ and $D_{wij} = \int_x K_{wij}(\mathbf{x})d\mathbf{x}$. Note that $C_{wij} \leq D_{wij}$. We refer to equations of this form as continuous state models.

Here, we have derived these relations using thermodynamics and equilibrium constants. A similar derivation for enzyme saturation is done in ref *44* using statistical mechanics. It is not hard to generalize from eq 35 presented in ref *44* to the continuous state model.

Since the assumptions that led to eq 8 (steady-state, pseudo first-order kinetics) are often very closely approximated in experiment, the continuous state model provides an error estimate. The data are fit (in a least-squares sense) with the proper continuous state model, and the deviation from each point is the approximate error. Assuming that steady-state and first-order kinetics are exactly satisfied, this will be a minimum error estimate since the correct model (with the actual error) need not be the least-squares optimum, though it should be close.

From eq 8, we can see that the number of free parameters to specify the model is $(q + 1)(r + 1)s + (q + 1)(r + 1)(s + 1) - 1$. This number is useful when more restricted models are used to fit the data. For example, if a discrete state model (a model that assumes an enzyme spends most of its time in a few conformations) is used to fit the data and that model has more free parameters than the appropriate continuous state model, then the two models are indistinguishable. Thus, the number of free parameters in the continuous state model provides an upper bound to the number of free parameters in more restrictive models.

Equation 8 can give a great deal of insight into enzyme function. It can show how many different binding sites exist on the enzyme for a particular substrate or effector. It can show whether a particular effector is an inhibitor or activator under different situations (regardless of the action of the inhibitor: competitive, noncompetetive, uncompetetive, etc.). However, it does not take advantage of the fact that a particular enzyme may spend most of its time in a few conformations. Thus, we cannot get much information from each coefficient, C_{wij} or D_{wij}.

5. APPENDIX B

Here, we consider a two-state model with activator and substrate for simplicity, though we used both a two-state and a three-state model. We use the standard notation of Monod et al., where the less active (Taut) conformation of the enzyme is denoted by *T* and the more active (Relaxed) by *R* (*20*). The rate constant for the reaction of substrate to product is denoted by k_R for the *R* state and k_T for the *T* state, with $k_R > k_T$.

The velocity of the reaction is the concentration of all of the *R* protomers (again using the terminology of Monod et al. for a single monomer) bound to substrate times k_R, and the concentration of all of the *T* protomers bound to substrate times k_T. To get activity, we divide by V^t_{max}, which was defined earlier (eq 4) as $sk_R[E]_0$ with $[E]_0$ being the initial concentration of the enzyme (i.e., the total concentration of enzyme in solution) and *s* the number of substrate binding sites.

In the KNF model, each protomer can exist in a *T* or *R* state. Furthermore, there is an interaction energy between like and unlike protomers. The dissociation constants that each ligand has for each state must be specified (in a two-state model with an activator and a substrate, this would be four parameters), as must the ratio of the rate constants for the two states, the interaction energy between like and unlike protomers (three combinations, but one can be the reference energy), and the equilibrium constant between the two states (*21*). This gives a total of $4 + 1 + 2 + 1$ or eight parameters to specify this simple model.

In the MWC model, however, the interaction energy between two unlike subunits is assumed to be large. Therefore, state transitions are concerted in that when one protomer changes state, the other protomer also changes nearly instantaneously. It might seem contradictory that we assume rapid steady-state and concerted transitions. If the state with unlike protomers has a very high free energy (comparable to the free energy barrier for turning reactant into product), then rapid steady state is no longer a good assumption because any state transition would occur on the same time scale as that of the total reaction. However, we need only assume that the free energy barrier is large enough to make the *TR* state have a negligible contribution to the activity of the enzyme. Assuming precisely concerted transitions is a conceptual simplification. With this assumption, we get rid of two parameters: we no longer have to specify the interaction energy between unlike subunits, and we can lump the interaction energy between like subunits in with the energy of state transitions. Thus, we need six parameters to specify this simple model.

For the simplest discrete state model, assuming only two ligands (AMP and substrate), AMP binding only to the allosteric effector site and concerted state transitions, the following reaction building blocks can then be defined and a model assembled from them:

$$T + A \overset{K_{TA_a}[A]}{\rightleftharpoons} TA \quad T + S \overset{K_{TS}[S]}{\rightleftharpoons} TS \quad TS \xrightarrow{k_T} T + P$$

$$R + A \overset{K_{RA_a}[A]}{\rightleftharpoons} RA \quad R + S \overset{K_{RS}[S]}{\rightleftharpoons} RS \quad RS \xrightarrow{k_R} R + P$$

$$T \overset{k_R}{\rightleftharpoons} R \qquad (9)$$

In these equations, each *K* represents an equilibrium constant. In these equations and throughout the article, each

T or *R* represents an individual protomer, *A* represents AMP, *a* indicates binding at the allosteric activator site, *S* represents substrate, and *P* represents product (either phosphate (P_i) or glucose-1-phosphate (G1P) depending on direction). Later, when we consider additional binding sites and additional effectors, we denote the nucleoside site by *i* and ATP by *I*. Thus, the equilibrium constant for binding ATP to the allosteric activator site in the *T* state would be K_{TIa}. In all of our models, we assumed that $k_T = 0$ because there is essentially zero activity for GPb in the absence of AMP.

For a two-state MWC model for a dimeric enzyme with 2 active sites binding substrate and 2 activator binding sites (the allosteric effector sites), we can assemble a kinetic model from these reaction building blocks given two assumptions. First, we assume that ligand concentrations change slowly with time. Second, we assume that the reactions are in equilibrium, with the exception of product formation (in other words, the rate of ligand binding/unbinding and enzyme configuration changes are fast with respect to product formation and release).

Alternatively, instead of this equilibrium assumption, we could assume that the system is in steady state and that the enzyme can only change configuration when it is free of ligand. With this steady-state assumption, the equilibrium constant $K_{RS} = k_{rs}^{+}/k_{rs}^{-}$ becomes an equivalent equilibrium constant $K'_{RS} = k_{rs}^{+}/(k_{rs}^{-} + k_R)$, and the following equations and kinetic diagrams are correct.

With the above assumptions (constant substrate/effector concentrations, equilibrium), we may define a simple mathematical model from the elementary reactions listed in eq 9. We then get the reaction scheme drawn in Figure 4, where each *K* is an equilibrium constant as defined in eq 9.

We then write the following expression for activity:

$$\frac{v}{V_{max}^{t}} = \frac{2K_{TR}\,(1 + K_{RA_a}\,[A])^2\,(K_{RS}[S] + K_{RS}{}^2\,[S]^2)}{2\,(1 + K_{TA_a}\,[A])^2\,(1 + K_{TS}\,[S])^2 + K_{TR}\,(1 + K_{RA_a}\,[A])^2\,(1 + K_{RS}\,[S])^2} \quad (10)$$

Note that this equation is of the form of eq 8, but the coefficients are no longer independent, being combinations of rate constants and equilibrium constants. The appropriate form of the model in eq 8 has 14 free parameters, the two-state KNF model has 7, and this two-state MWC model has 5.

This equation holds for a two-state MWC model with one substrate binding site and one allosteric AMP binding site per protomer. We also consider a two-state KNF model, a three-state MWC model, and ATP and AMP binding to the inhibitory nucleoside site. The addition of a state or of a new effector binding site changes the above model in simple predictable ways, but the equations become large and cumbersome and are not worth reproducing here.

It is not possible to represent all of the inactive states with one average state because the increasing number of free parameters that an extra state affords removes some of the constraints in the discrete state model and makes it more closely approach the continuous state model. Looking at eq 10, we see that the addition of a second inactive state adds two new parameters in the denominator but still does not completely span the space of polynomials second order in [*A*] and [*S*]. In fact, it can be shown that three inactive states completely span the space so that any more than three inactive states have no effect on the model. If we increase the degree of the denominator polynomial, such as by allowing an extra effector to bind to the enzyme or by adding an additional binding site for an existing effector, we increase the number of inactive states that we can add before the polynomial space is spanned. The upper bound in the number of parameters is given by the number of free parameters in the continuous state model.

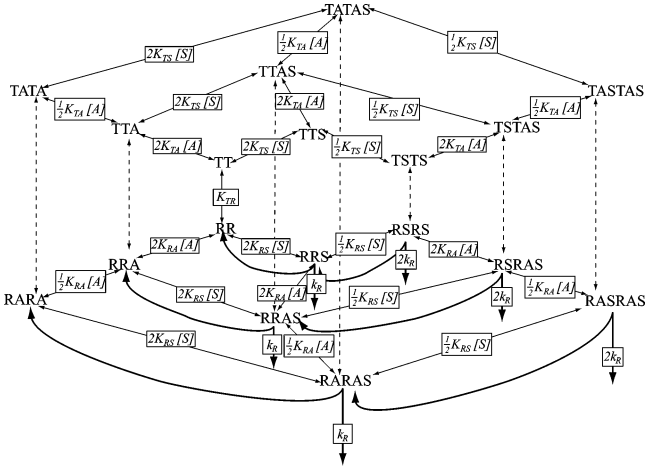

FIGURE 4: Kinetic scheme for a simple two state MWC model of an enzyme that binds two molecules of substrate, *S*, and activator, *A*. Each potential chemical reaction is shown by a double-headed arrow and a box containing an equilibrium constant. This equilibrium constant represents the ratio of the concentration of the chemical species with more ligand bound to the chemical species with less ligand bound (e.g., $2K_{TS}[S] = [TTS]/[TT]$) or the ratio of chemical species in the *R* state to the chemical species in the *T* state (e.g., $K_{TR} = [RR]/[TT]$). The equilibrium constants for the unlabeled arrows (vertical, dashed) can be found from the other equilibrium constants, for example, $[RRS]/[TTS] = K_{TR}K_{RS}/K_{TS}$.

6. APPENDIX C

Sergienko and Srivastava provide an excellent data set for the reaction velocity in the direction of glycogen synthesis at 25 °C (*17*). They collected data over variable AMP at six levels of G1P and variable G1P at six levels of AMP. Their measurements are more accurate than previous work because of a newly developed technique (*23*).

We used Lowry et al. (*13*) for the 25 °C data in the direction of glycogen breakdown (left to right in eq 1). These data were not all collected under saturating levels of glycogen, which posed a potential problem, since we did not wish to include the additional variable of glycogen kinetics into our model. However, a glycogen concentration of 7−10 mM is approximately saturating; therefore, we were able to use about half of their data for our fits, which made the data set relatively small. Activity was measured at several constant levels of P_i while varying AMP as well as at several constant levels of AMP while varying P_i. Unfortunately, the variable AMP data were collected at 26 °C, while the variable P_i data were collected at 23 °C. Thus, there were probably temperature differences between the two experiments, and our best-fit parameters likely represent an average of the parameters for the two cases.

Madsen and Shechosky provide a large data set both in the direction of glycogen breakdown and synthesis, collected

at 30 °C (*12*). This data set has the additional benefit that the concentration of ATP is varied.

We used Klinov and Kurganov for the 30 °C data in the direction of glycogen synthesis (*18*). The data set is large and covers a wide range of AMP using the modern measuring technique (*23*). However, it only has three different levels of G1P. The large range of AMP leads to the unphysiological situation where AMP inhibition must be considered. Fitting data with AMP inhibition allows us to ensure that it does not happen under physiological conditions. They reported a 3% error, which allowed us to validate our error-estimation technique.

ACKNOWLEDGMENT

We are very grateful to Dr. David Cabrera for help on the optimizations and Dr. Brian Crane for suggestions on the manuscript.

REFERENCES

1. Cori, G. T., Colowick, S. P., and Cori, C. F (1938) The action of nucleotides in the disruptive phosphorylation of glycogen, *J. Biol. Chem. 123*, 381−389.
2. Shulman, R. G., and Rothman, D. L. (2001) The "glycogen shunt" in exercising muscle: a role for glycogen in muscle energetics and fatigue, *Proc. Natl. Acad. Sci. U.S.A. 98*, 457−461.
3. Lambeth, M. J., and Kushmerick, M. J. (2002) A computational model for glycogenolysis in skeletal muscle, *Ann. Biomed. Eng. 30*, 808−827.
4. Lu, Z., Bohn, J., Bergeron, R., Deng, Q., Ellsworth, K. P., Geissler, W. M., Harris, G., McCann, P. E., McKeever, B., Myers, R. W., Saperstein, R., Willoughby, C. A., Yao, J., and Chapman, K. (2003) A new class of glycogen phosphorylase inhibitors, *Bioorg. Med. Chem. Lett. 13*, 4125−4128.
5. Kristiansen, M., Anderson, B., Iverson, L. F., and Westergaard, N. (2004) Identification, synthesis and characterization of new glycogen phosphorylase inhibitors binding to the allosteric AMP site, *J. Med. Chem. 47*, 3537−3545.
6. Cardenas, M. L., and Goldbeter, A. (1996) The glucose-induced switch between glycogen phosphorylase and glycogen synthase in the liver: outlines of a theoretical approach, *J. Theor. Biol. 182*, 421−426.
7. Mutalik, V. K., and Venkatesh, K. V. (2005) Quantification of the glycogen cascade system: the ultra-sensitive responses of liver glycogen synthase and muscle phosphorylase are due to distinctive regulatory designs, *Theor. Biol. Med. Model. 2*, 19.
8. Johnson, L. N. (1992) Glycogen phosphorylase: control by phophorylation and allosteric effectors, *FASEB J. 6*, 2274−2282.
9. Madsen, N. B. (1964) Allosteric properties of phosphorylase b, *Biochem. Biophys. Res. Commun. 15*, 390−395.
10. Morgan, H. E., and Parmeggiani, A. (1964) Regulation of glycogenolysis in muscle III: control of muscle glycogen phosphorylase activity, *J. Biol. Chem. 239*, 2440−2445.
11. Helmreich, E., and Cori, C. F. (1964) The role of adenylic acid in the activation of phosphorylase, *Proc. Natl. Acad. Sci. U.S.A. 51*, 131−138.
12. Madsen, N. B., and Shechosky, S. (1967) Allosteric properties of phosphorylase b II: comparison with a kinetic model, *J. Biol. Chem. 242*, 3301−3307.
13. Lowry, O. H., Schulz, D. W., and Passoneau, J. V. (1967) The kinetics of glycogen phosphorylase from brain and muscle, *J. Biol. Chem. 242*, 271−280.
14. Engers, H. D., and Madsen, N. B. (1968) The effect of anions on the activity of phosphorylase b, *Biochem. Biophys. Res. Commun. 33*, 49−54.
15. Kastenschmidt, L. L., Kastenschmidt, J., and Helmreich, E. (1968) The effect of temperature on allosteric transitions in rabbit skeletal muscle phosphorylase b, *Biochemistry 7*, 4543−4556.
16. Klinov, S. V, and Kurganov, B. I. (1994) Kinetic mechanism of activation of muscle glycogen phosphorylase b by adenosine 5′-monophosphate, *Arch. Biochem. Biophys. 312*, 14−21.
17. Sergienko, E. A., and Srivastava, D. K. (1997) Kinetic mechanism of the glycogen-phosphorylase-catalyzed reaction in the direction of glycogen synthesis: co-operative interactions of AMP and glucose-1-phosphate during catalysis, *Biochem. J. 328*, 83−91.
18. Klinov, S. V, and Kurganov, B. I. (2001) Combined kinetic mechanism describing activation and inhibition of muscle glycogen phosphorylase b by adenosine 5′-monophosphate, *Biophys. Chem. 92*, 89−102.
19. Dill, K. A., and Bromberg, S. (2003) *Molecular Driving Forces: Statistical Thermodynamics in Chemistry and Biology*, Garland Science, Taylor and Francis Group, Oxford, U.K.
20. Monod, J., Wyman, J., and Changeux, J-P. (1965) On the nature of allosteric transitions: a plausible model, *J. Mol. Biol. 12*, 88−118.
21. Koshland, D. K., Neméthy, S., and Filmer, D. (1966) Comparison of experimental data and theoretical models in proteins containing subunits, *Biochemistry 5*, 365−386.
22. Doornik, J. A. and Hansen, H. (1994) *An Omnibus Test for Univariate and Multivariate Normality* (Economics Group, Nuffield College, University of Oxford) Technical Report W4&91, available at http://ideas.repec.org/p/nuf/econwp/9604.html.
23. Sergienko, E. A., and Srivastava, D. K. (1994) A continuous spectrophotometric method for the determination of glycogen phosphorylase-catalyzed reaction in the direction of glycogen synthesis, *Anal. Biochem. 221*, 348−355.
24. Buchbinder, J. L., and Fletterick, R. J. (1996) Role of active state gate of glycogen phosphorylase in allosteric inhibition and substrate binding, *J. Biol. Chem. 271*, 22305−22309.
25. Kasvinsky, P. J., Madsen, N. B., Sygusch, J., and Fletterick, R. J. (1978) The regulation of phosphorylase a by nucleotide derivatives, *J. Biol. Chem. 253*, 3343−3351.
26. Wang, Z. X. (1999) Influence of substrates on *in vitro* dephosphorylation of glycogen phosphorylase a by protein phosphatase-1, *Biochem. J. 341*, 545−554.
27. Newgard, C. B., Hwang, P. K., and Fletterick, R. J. (1989) The family of glycogen phosphorylases: structure and function, *Crit. Rev. Biochem. Mol. Biol. 24*, 69−99.
28. Griffiths, J. R., Price, N. C., and Radda, G. K. (1974) Conformational changes in phosphorylase a, studied by a spin labeled probe, *Biochim. Biophys. Acta 358*, 275−280.
29. Barford, D., and Johnson, L. N. (1989) The allosteric transition of glycogen phosphorylase, *Nature 340*, 609−616.
30. Battersby, M. K., and Radda, G. K. (1979) Intersubunit transition of ligan effects in the glycogen phosphorylase b dimer, *Biochemistry 18*, 3774−3780.
31. Madsen, N. B. (1986) *Glycogen Phosphorylase* (Boyer, P. D., and Krebs, E. G., Eds.) Vol. 17, pp 365−394, Academic Press, New York.
32. Busby, S. J. W., and Radda, G. K. (1976) Regulation of the glycogen phosphorylase system: from physical measurements to biological speculations, *Curr. Top. Cell. Regul. 10*, 89−160.
33. Johnson, L. N., Stura, E. A., Wilson, K. S., Sansom, M. S. P., and Weber, I. T. (1979) Nucleotide binding to glycogen phosphorylase b in the crystal, *J. Mol. Biol. 134*, 639−653.
34. Sprang, S., Goldsmith, E., and Fletterick, R. (1987) Structure of the nucleotide activation switch in glycogen phosphorylase a, *Science 237*, 1012−1019.
35. Rush, J. W. E., and Spriet, L. L. (2001) Skeletal muscle glycogen phosphorylase a kinetics: effects of adenine nucleotides and caffeine, *J. Appl. Physiol. 91*, 2071−2078.
36. Danforth, W. H., and Lyon, J. B., Jr. (1964) Glycogenolysis during tetanic contraction fo isolated mouse muscles in the presence and absence of phosphorylase a, *J. Biol. Chem. 12*, 4047−4050.
37. Katz, A., Andersson, D. C., Yu, J., Norman, B., Sandstrom, M. E., Wieringa, B., and Westerblad, H. (2003) Contraction-mediated glycogenolysis in mouse skeletal muscle lacking creatine kinase: the role of phosphorylase b activation, *J. Physiol. 553*, 523−531.
38. Cleland, W. W. (1963) The kinetics of enzyme-catalyzed reactions with two or more substrates of products I. Nomenclature and rate equations, *Biochim. Biophys. Acta 67*, 104−137.
39. Edsall, J. T., and Wyman, J. (1958) *Biophysical Chemistry*, Academic Press, New York.
40. Wong, J. T., and Hanes, C. S. (1962) Kinetic formulations for enzymic reactions involving two substrates, *Can. J. Biochem. Physiol. 40*, 763−804.
41. Bardsley, W. G., and Childs, R. E. (1975) Sigmoid curves, nonlinear double reciprocal plots and allosterism, *Biochem. J. 149*, 313−328.

42. Childs, R. E., and Bardsley, W. G. (1975) Allosteric and related phenomena: an analysis of sigmoid and non-hyperbolic functions, *J. Theor. Biol. 50*, 45−58.
43. Wyman, J. and Gill, S. J. (1990) *Binding and Linkage: Functional Chemistry of Biological Macromolecules*, University Science Books, New York.
44. Wang, Z. X. (1990) Some applications of statistical mechanics in enzymology I: elementary principle, *J. Theor. Biol. 143*, 445−455.

BI7005527